XLVI CILAMCE
VITÓRIA - ES - BRAZIL - 2025
XLVI IBERO-LATIN AMERICAN CONGRESS ON COMPUTATIONAL METHODS IN ENGINEERING

Dynamic Behavior of the Vehicle Body in an Automobile Equipped with Magnetorheological Dampers

Luiz F. B. de Palma[1], Ricardo T. C. Neto[1], Guilherme B. R. Conrado[1], Gabrielle B. Rangel[1]

[1]*Dept. of Mechanical Engineering, Military Institute of Engineering*
Praça Gen. Tibúrcio, 80, 22290-270, Rio de Janeiro/RJ, Brazil
ricardo@ime.eb.br, guibrconrado@ime.eb.br, bonellagabrielle@gmail.com

Abstract. The application of magnetorheological (MR) dampers has materially enhanced the safety of both passenger and heavy-duty vehicles. In this framework, the present work introduces a vehicle model, implemented within the MATLAB/Simulink® environment, whose suspension system is equipped with MR-dampers, in which vertical and longitudinal dynamics are intrinsically coupled. The MR-dampers are characterized by a hyperbolic tangent function incorporating a hysteresis component and are individually regulated via a Sugeno-type fuzzy control schema. Longitudinal tire forces are computed using the Modified Burckhardt model. The primary objective is to assess the vehicle-body response while traversing uneven terrain at velocities that generate high base-excitation frequencies. The MR-damping system exhibited superior performance in all scenarios compared to conventional linear damping, although the computational cost was relatively high, primarily due to the controller's performance being highly sensitive to variations in the model parameters. The change of the Simulink integration method from *ode15* to *ode45*, without imposing a maximum step size constraint, resulted in a reduction of the simulation runtime.

Keywords: Power Flow, Longitudinal Vehicle Dynamics, Vertical Vehicle Dynamics, Magnetorheological Damper, Block Diagram.

1 Introduction

In this work, the dynamics of a vehicle are coupled to enable the evaluation of the influence of vertical load on each wheel on the corresponding longitudinal tire force. The model is implemented as a block diagram for simulation in MATLAB/Simulink®, representing an evolution of the model developed by [1]. The modeling methodology follows the power flow approach [2], which ensures system modularity since each block operates independently of the others. The tires are modeled using the Modified Burckhardt model [3] for longitudinal dynamics, and are considered as linear springs for vertical dynamic calculations. The suspension system does not include the detailed mechanical configuration; instead, it consists of a linear spring-damper pair, which may be replaced by a magnetorheological (MR) damper.

The vehicle body is considered a rigid body with four degrees of freedom (DOF): bounce, pitch, roll, and longitudinal translation (X-direction). Each wheel has 2 DOF: spin and hop, leading to a total of 12 DOF. The brake system is hydraulic [1], with disc brakes on all four wheels. To investigate the damping effect, a mathematical model of a magnetorheological damper is introduced [4, 5, 6]. In order to compare the performance of these suspension components, a computational simulation was conducted between two otherwise identical vehicles differing only in their dampers. The dynamic response of the vehicle body was compared in each case. This approach highlights the advantage of the modularity enabled by the power flow-based modeling framework.

2 Vehicle Model

The architecture of the mathematical model is presented in Fig. 1. Each block contains the corresponding equations. The adopted Cartesian coordinate system follows the ISO 8855 standard [7], with the origin of the vehicle body reference frame located at its center of mass.

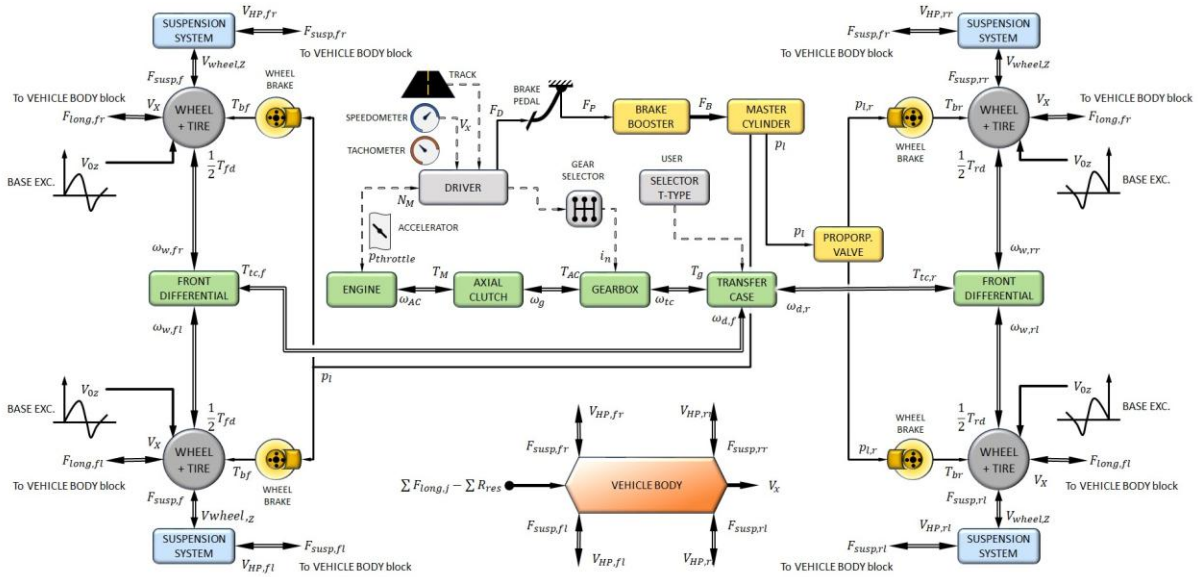


Figure 1. Vehicle mathematical model in block diagram form

2.1 Vehicle Body

The vehicle body is modeled as a rigid body with six degrees of freedom (6-DOF), of which two, lateral displacement and yaw, are constrained. This constraint is implemented within the block diagram, where the corresponding accelerations, as calculated by the equations of motion, are set to zero. The coordinate transformation matrix from the vehicle body reference frame to the body-fixed frame, eq. (1), is derived using the 3-2-1 rotation sequence [8], where φ denotes the roll angle, θ the pitch angle, and ψ the yaw angle.

$$ {}^{f}\mathbf{T}^{c} = \begin{bmatrix} \cos\theta\cos\psi & (\sin\phi\sin\theta\cos\psi - \cos\phi\sin\psi) & (\cos\phi\sin\theta\cos\psi + \sin\phi\sin\psi) \\ \cos\theta\sin\psi & (\sin\phi\sin\theta\sin\psi + \cos\phi\cos\psi) & (\cos\phi\sin\theta\sin\psi - \sin\phi\cos\psi) \\ -\sin\theta & \sin\phi\cos\theta & \cos\phi\cos\theta \end{bmatrix} \tag{1} $$

The $\dot{\phi}$, $\dot{\theta}$, and $\dot{\psi}$ values are computed from the angular velocity vector of the vehicle body, expressed in its own reference frame, as shown in eq. (2), using the transformation matrix $\mathbf{G}$. These values are then integrated and used to update the coordinate transformation matrix at each simulation time step. The angular velocity vector ${}^{c}\boldsymbol{\Omega}_{b}$ is determined using the Euler equation of motion for the vehicle body, formulated in its body-fixed reference frame c (eq. 3a), whereas the Newton equation of motion (eq. 3b) is expressed in the inertial reference frame f.

$$ \begin{bmatrix} \dot{\phi} \\ \dot{\theta} \\ \dot{\psi} \end{bmatrix} = \begin{bmatrix} 1 & (\sin\phi\tan\theta) & (\cos\phi\tan\theta) \\ 0 & \cos\phi & -\sin\phi \\ 0 & (\sin\phi/\cos\theta) & (\cos\phi/\cos\theta) \end{bmatrix} {}^{c}\boldsymbol{\Omega}_{b} = \mathbf{G}\ {}^{c}\boldsymbol{\Omega}_{b} \tag{2} $$

$$ {}^{c}\dot{\boldsymbol{\Omega}}_{b} = {}^{c}\mathbf{J}_{b}^{-1}\left({}^{c}\mathbf{n}_{C,susp} + {}^{c}\mathbf{n}_{C,tires} - {}^{c}\tilde{\boldsymbol{\Omega}}_{b}\ {}^{c}\mathbf{J}_{b}\ {}^{c}\boldsymbol{\Omega}_{b} \right) \tag{3a} $$

$$ {}^{f}\dot{\mathbf{v}}_{C} = \mathbf{M}_{b}^{-1}\left(\sum {}^{f}\mathbf{F}_{j} + \mathbf{W}_{b} \right) \tag{3b} $$

where,

${}^{c}\boldsymbol{\Omega}_{b}$ – angular velocity vector of the vehicle body;

${}^{\mathrm{f}}\dot{\mathbf{v}}_{\mathrm{C}}$ – linear velocity vector of the vehicle body's center of gravity

${}^{c}\mathbf{J}_{\mathrm{b}}$ – inertia tensor of the vehicle body;

$\mathbf{M}_{b}$ – vehicle body's mass matrix, $diag([m_b \quad m_b \quad m_b]^{\mathrm{t}})$;

${}^{c}\mathbf{n}_{C,susp}$ – resultant moment applied at the vehicle body's center of gravity (from suspensions);

${}^{c}\mathbf{n}_{C,tires}$ – resultant moment applied at the vehicle body's center of gravity (from tires);

$\sum {}^{f}\mathbf{F}_{j}$ – resultant of the forces applied at the vehicle body's center of gravity;

$\mathbf{W}_{b}$ – vehicle body's weight vector, $[0 \quad 0 \quad -m_b g]^{\mathrm{t}}$.

The velocities of the vehicle body's degrees of freedom are related to the velocities of the suspension hardpoints through the kinematic constraint matrix, eq. (4), which is derived from the vector equations [2], eq. (5):

$$\begin{bmatrix} \vdots \\ {}^{f}\mathbf{v}_{HPj} \\ \vdots \end{bmatrix} = \boldsymbol{\Theta}_{b} \begin{bmatrix} {}^{f}\mathbf{v}_{C} \\ {}^{c}\boldsymbol{\Omega}_{b} \end{bmatrix} \tag{4}$$

$$\boldsymbol{\Theta}_{b} = \begin{bmatrix} \mathbf{I}_{3} & \\ \vdots & \\ -{}^{f}\mathbf{T}^{c}\,{}^{c}_{C}\tilde{\mathbf{r}}_{HPj} & \\ \vdots & \end{bmatrix} \tag{5}$$

where, ${}^{c}_{C}\mathbf{r}_{HPj}$ is the position vector from point *C* to point HP_j expressed in the body reference frame, and $\mathbf{I}_3$ is the identity matrix. The transpose of the matrix $\boldsymbol{\Theta}_{b}$ transfers the forces applied at the points *HPj* to the vehicle body's center of mass, *C*, along with the corresponding equivalent moments, as shown in eq. (6):

$$\begin{bmatrix} \sum {}^{f}\mathbf{F}_{j} \\ {}^{c}\mathbf{n}_{C,susp} \end{bmatrix} = \boldsymbol{\Theta}_{b}^{\mathrm{t}} \begin{bmatrix} \vdots \\ {}^{f}\mathbf{F}_{HPj} \\ \vdots \end{bmatrix} \tag{6}$$

where ${}^{\mathrm{f}}\mathbf{F}_{\mathrm{HPj}} = \left[{}^{f}F_{HPj,x} \quad 0 \quad {}^{f}F_{HPj,z} \right]^{\mathrm{t}}$ is the force vector applied at point HP_j. These forces are generated by the suspensions (${}^{f}F_{HPj,z}$) and the tires (${}^{f}F_{HPj,x}$).

2.2 Vehicle Suspensions

The vehicle's suspensions consist only of elastic elements, a pair of linear springs (Hooke's law), and a viscous damper, with no specific mechanical configuration adopted. Since the input to each suspension block is the velocity of the corresponding hardpoints at the vehicle body and the wheel's center of gravity (CG), the relative velocity is computed. This velocity is used to calculate both the force produced by the damper and the force developed by the spring. Given that both the spring and damper undergo the same displacement, the magnitude of the force developed by the conventional passive elements is expressed in eq. (7).

$$F_{S,j} = b_{s,j}\left({}^{f}v_{Wj,z} - {}^{f}v_{HPj,z} \right) + b_{s,j} \int \left({}^{f}v_{Wj,z} - {}^{f}v_{HPj,z} \right) dt \tag{7}$$

where, $b_{s,j}$ is the damper viscous coefficient, $k_{s,j}$ the spring stiffness coefficient, ${}^{f}v_{Wj,z}$ the z-component of the

wheel CG's velocity, ${}^{f}v_{HPj,z}$ the z-component of the body's hardpoint velocity. The block diagram is show at Fig. 2a. The conventional viscous damper can be replaced by a magnetorheological one in each suspension (Fig. 2b). Each magnetorheological damper has its own controller. The model chosen is the *hyperbolic tangent* presented in [9], eq. (8a).:

$$F_{d-MR,j} = b_{s,j}\dot{\delta}_j + k_{ds,j}\delta_j + \alpha \tanh\left(\beta\dot{\delta}_j + \delta_j\right) + f_0 \tag{8a}$$

where,

$$b_{s,j} = 2100 i_{MR} + 1232 \tag{8b}$$

$$k_{ds,j} = -1700 i_{MR} + 5100 \tag{8c}$$

$$\alpha = -244 i_{MR}^2 + 918 i_{MR} + 32 \tag{8d}$$

$$\beta = 120 \tag{8e}$$

$$f_0 = -18 i_{MR} - 257 \tag{8f}$$

where, δ_j is the relative displacement between the ends, $b_{s,j}$ the damper viscous coefficient, $k_{ds,j}$ the damper stiffness coefficient, α the scale factor of the hysteresis, β the hysteresis gradient parameter, and f_0 is the damper force offset. i_{MR} is the electric current flowing through the coil of the MR-damper.

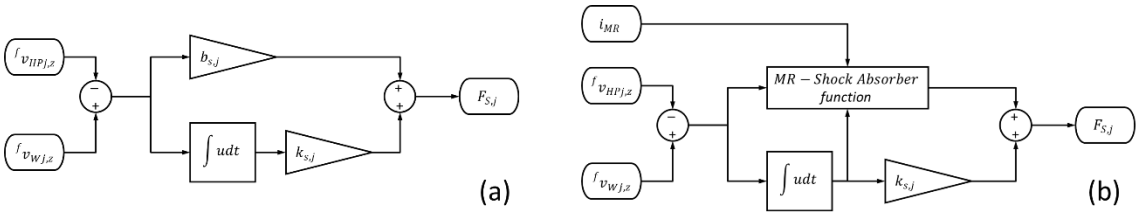


Figure 2. Suspension block. (a) With a conventional damper, (b) with an MR-damper.

2.3 MR-damper controller

To handle the model's nonlinearities with a less robust implementation, a Fuzzy Logic controller is adopted. This type of control system is capable of interpreting various inputs from nonlinear systems without requiring a detailed or highly robust mathematical model [5,6]. The MATLAB® Fuzzy Logic Toolbox is used to implement the zero-order Sugeno inference method, in which the fuzzy output corresponds to the control current, represented by five singleton membership functions evenly distributed between zero and one.

2.4 Wheels and tires

Each WHEEL+TIRES block contains two equations of motion: an Euler equation, used to compute the angular acceleration of the wheel's spin motion [1], and a Newton equation, used to calculate the vertical velocity. The tire is modeled as a linear spring according to Hooke's Law, with no damping effect, and the vertical dynamics are computed assuming a single contact point.

3 Implementation of the Controller Using MATLAB/Simulink®

Fuzzy logic behavior in Simulink systems: The fuzzy logic controller implemented in Simulink behaves similarly to a single-layer feedforward neural network, mapping input variables directly to outputs through membership functions and a rule base. This system is inherently static, lacking temporal dynamics or internal

memory, and therefore produces immediate responses based solely on current input values. In contrast, a vehicle plant model in Simulink exhibits physical inertia and dynamic behavior, responding to input changes with natural delays. As a result, discontinuities in fuzzy outputs, such as abrupt rule switching, are not immediately reflected in the vehicle response, instead producing transient phenomena or oscillations depending on the controller's tuning.

Strategies to address input range and discontinuities: when input signals fall outside the predefined fuzzy inference system (FIS) range, no rules are activated, and the output defaults to a fixed average value, introducing undesirable discontinuities. One corrective strategy is to broaden the input range of the FIS, allowing for greater signal variability, though this may reduce local sensitivity and dilute control precision. An alternative, more targeted approach involves adjusting the gain of input signals before they reach the fuzzy block. By scaling inputs to fit within the FIS's active range, this method preserves the original membership function structure and inference consistency, preventing discontinuities and maintaining effective fuzzy control behavior.

The controller is a zero-order Sugeno type, in which the outputs are related to the inputs through constant values [4, 5, 6]. The output current is normalized within the range of 0 to 1. The fuzzy rule set is presented in Table 1. The control is applied at each chassis point i, as a function of the relative velocity between the chassis anchoring point and the damper, xi_1, the velocity of the chassis anchoring point, xi_2, and its acceleration, xi_3. To ensure compatibility of each variable with the universe of discourse, the input values are multiplied by a gain before the fuzzification process [6].

Table 1. Fuzzy rules.

x_{i3}	N			Z			P		
x_{i1}/x_{i2}	N	Z	P	N	Z	P	N	Z	P
N	i5	i4	i2	i4	i1	i1	i3	i1	i1
Z	i1	i1	i1	i1	i1	i1	i1	i1	i1
P	i1	i1	i3	i1	i1	i4	i2	i4	i5

The output current is normalized within a range from 0 to 1, therefore i1 = 0, i2 = 0.25, i3 = 0.5, i4 = 0.75, and i5 = 1. Both the inputs and outputs are weighted to match the problem data with the value range of the fuzzification process (Fig. 3). The gains applied in the controller are $G_x = 1/3$ (relative velocity gain), $G_v = 0.25$ (absolute velocity gain), $G_a = 1/30$ (absolute acceleration gain coefficient), and $G_u = 6$. The variable G_u is used to modify the scale of the output variable (current i_{MR}) since the output of the fuzzy control is situated among the numbers zero and one. Therefore, the maximum current is limited to the value assigned to the variable G_u.

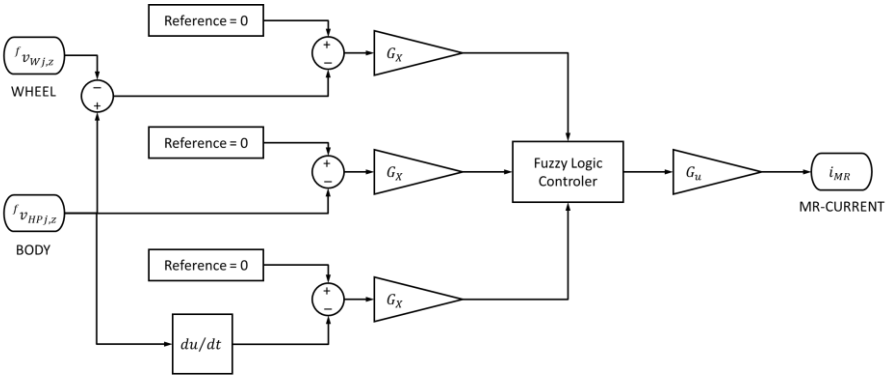


Figure 3. Block Diagram for the MR damper fuzzy controller.

4 Simulations and Results

To provide a better understanding of the differences between the MR- and conventional dampers, the force curves for each device are plotted, with the forces computed as a function of the piston velocity. A velocity range of [–1, 1] m/s was defined, which is typical for passenger vehicle suspensions. The conventional dampers are of the viscous type, following the constitutive relation represented by the first term of eq. (7), with front/rear damping coefficients of 980/1100 Ns/m. The expression for the MR-damper force is given by eq. (8a) [9]. The plots of the MR-damper current variation and the corresponding damping forces are shown in Fig. 4. In this case, the control system acting on the current was maintained.

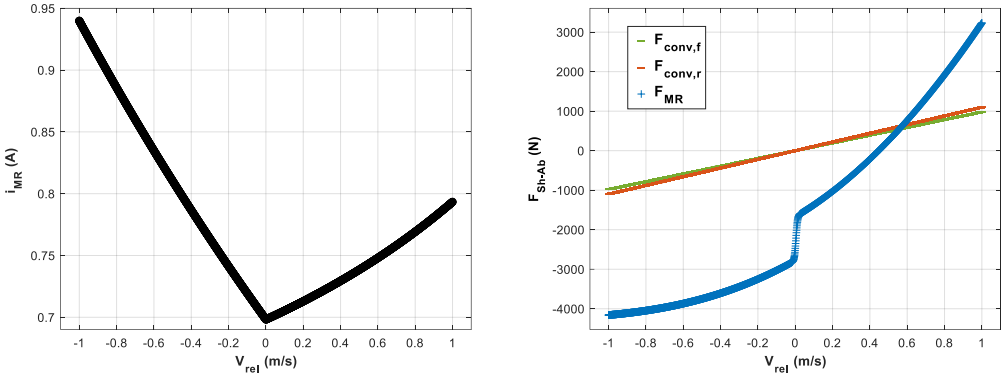


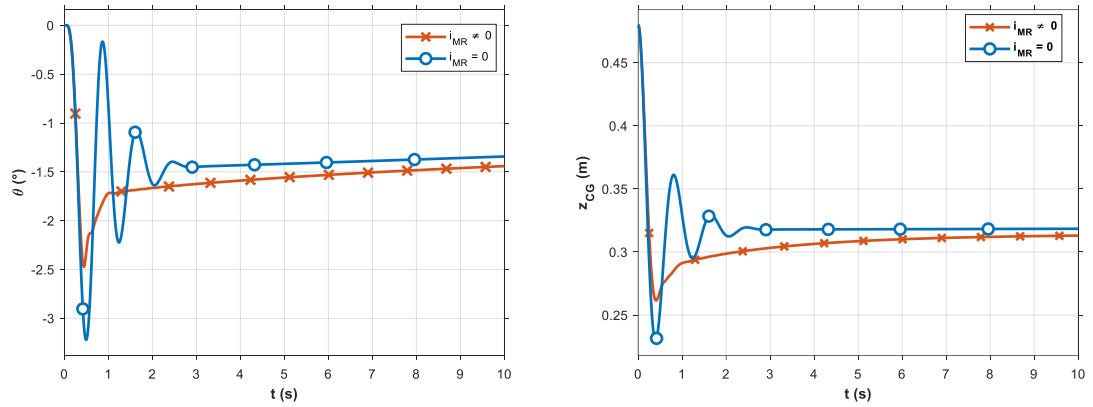
Figure 4. (a) current × piston velocity curve, (b) Force × piston velocity curve (front and rear conventional dampers are straight lines).

The expression in eq. (8a) [9] shows that the MR-damper includes a stiffness term represented by $k_{ds,j}$. In contrast, conventional dampers are linear and viscous. The MR-damper curve is nonzero when the piston velocity is zero due to the terms in eqs. (8c) and (8f). Therefore, it is expected that the steady-state position of the vehicle equipped with these dampers differs from that of the same vehicle when equipped with conventional dampers.

The vehicle is simulated starting from an initial speed of 10 km/h, progressively accelerating until it reaches maximum velocity on a dry concrete flat road surface. This speed is maintained until the pavement becomes irregular, after the vehicle has traveled a distance $s_{obs} = 10$ km. The obstacle consists of a sequence of 20 sinusoidal undulations (eq. 9), with an amplitude $H_{qm} = 0.05$ m, and a horizontal length $L_{qm} = 2.60$ m, where $j = 1$ refers to the front axle and $j = 2$ to the rear axle. a_j is the distance from the corresponding axle to the vehicle body's center of gravity (CG).

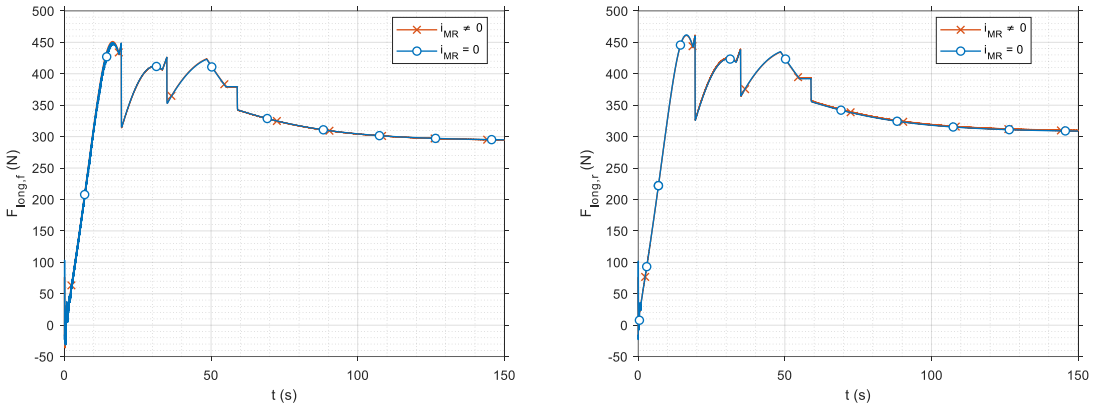
$$z_{0,j} = \left(H_{qm}/2\right)\left\{1 - \cos\left[\left(\pi/L_{qm}\right)\left(s_x(t) \pm a_j - s_{obs}\right)\right]\right\} \tag{9}$$

Figure 5 presents a comparison of the vehicle behavior with and without current applied to the MR-damper during the settling phase, as the vehicle slowly accelerates from the initial speed of 10 km/h. It is observed that the MR-damper reduces oscillations during the vertical body motion settling phase while the vehicle is accelerating. The behavior of the longitudinal forces on the front and rear axles is shown in Figs. 6a and 6b, respectively. The traction system is all-wheel drive (4×4). The discontinuities in the curves indicate gear shift events (from 1st to 4th gear). The forces developed at the rear axle tires are slightly higher than those at the front axle, due to dynamic weight transfer during acceleration. The magnetorheological damping does not influence the longitudinal forces.



(a) (b)

Figure 5. (a) body pitch behavior, (b) body's CG vertical position (zero MR-current and nonzero MR-current).



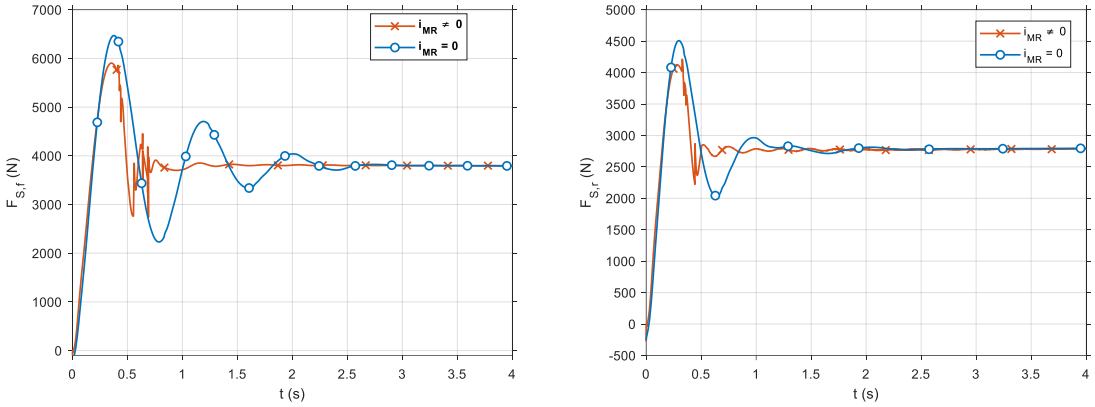
(a) (b)

Figure 6. Longitudinal forces developed by the tires (a) front axle, (b) rear axle.

Figure 7 shows the suspension force responses of the front axle (Fig. 7a) and the rear axle (Fig. 7b). The influence of the MR-damper is evident, as it reduces the vehicle body oscillations during the settling time. The suspension forces on the front axle are higher due to the static weight distribution (58% front, 42% rear). The vehicle body weighs 1343 kgf. After traversing the obstacle at a speed of 207 km/h (the maximum reached by the vehicle), the control system tends to reduce the vehicle body pitch (Fig. 8a) by adjusting the rear suspension forces to compensate for its inclination (Fig. 8b).

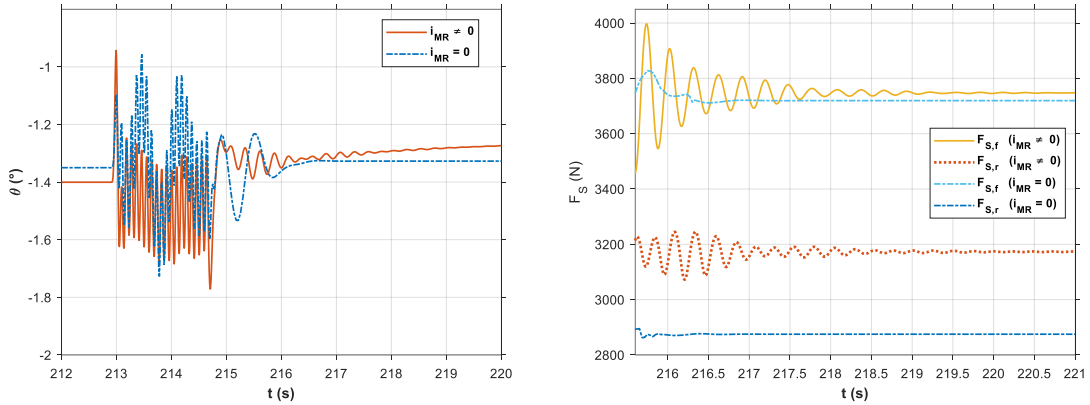
To evaluate the dynamic response of the adopted MR-damper model, a simulation was conducted in which the vehicle traverses a sinusoidal obstacle at its maximum speed of 207 km/h. The wavelength of the undulations was defined to yield an excitation frequency close to the resonance mode associated with predominant wheel motion (10.9 and 11.2 Hz), resulting in a horizontal length of 2.6 m per bump.

The MR-damper effectively reduced the vertical displacement of the wheel centers of gravity for both the front (Fig. 9a) and rear axles (Fig. 9b) during obstacle traversal. It is important to highlight that both minimum and maximum tire deformation limits were not implemented in the model.



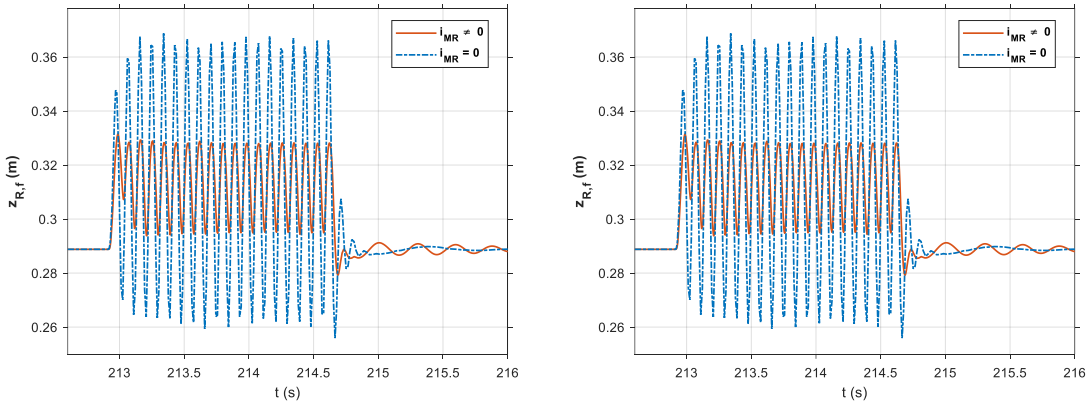
(a) (b)

Figure 7. Force of the suspensions. (a) Front axle, (b) rear axle.



(a) (b)

Figure 8. (a) Vehicle body pitch angle behavior; (b) variations in suspension forces.



(a) (b)

Figure 9. Vertical position variation of the (a) front- and (b) rear-axle wheels (dashed line $i_{MR} = 0$).

5 Conclusions

The block-structured mathematical model, due to its modular configuration, enables targeted modifications provided that causality is preserved throughout the system. This characteristic allows for the straightforward deactivation of the damper control logic by removing the corresponding control blocks (one controller box per damper) and nullifying the applied current, thereby rendering the magnetorheological (MR) dampers passive.

Simulations revealed no significant interference from the MR-damper on either the body dynamics or the longitudinal forces generated at the tire–road interface, which are governed by the vertical load, during gear-shifting events in the acceleration phase - starting from 10 km/h and reaching the vehicle's top speed of 207 km/h. These simulations were conducted on a dry concrete surface, and the Modified Burckhardt tire model exhibited notable numerical stability under such conditions.

Regarding the fuzzy logic-based control strategy, the computational time was found to significantly exceed the expected performance thresholds. This inefficiency is partially attributed to the static definition of the inference rules, which are not subject to automatic adaptation or learning. As such, a preliminary optimization procedure is required for proper calibration of the MR-current controller. In this work, the control objective was defined as the minimization of the vehicle body's pitch angle.

Although the controller effectively reduced body oscillations during the settling phase (from vehicle release to steady-state operation) and minimized the vertical displacements of the wheel centers of gravity during high-speed traversal of an uneven surface, the computational cost associated with the fuzzy control approach was deemed excessive. Additionally, in certain simulation scenarios, the controller failed to respond adequately to parameter variations, thereby requiring iterative retuning of control gains to ensure consistent performance.

Acknowledgements. The authors would like to thank the Mechanical Engineering Section (SE/4) of the Military Institute of Engineering for providing the resources and support necessary to carry out this work.

Authorship statement. The authors hereby confirm that they are the sole liable persons responsible for the authorship of this work, and that all material that has been herein included as part of the present paper is either the property (and authorship) of the authors, or has the permission of the owners to be included here.

References

[1] R. T. Costa Neto and B. R. Loiola. "Passenger vehicle behavior modeled by Power Flow using different mathematical tire models". *XLV Ibero-Latin American Congress on Computational Methods in Engineering*, (XLV CILAMCE, 2024), DOI: https://doi.org/10.55592/cilamce.v6i06.8084.

[2] R. T. Costa Neto, and M. Speranza Neto, "Elimination of algebraic loops in closed kinematic chains through power flow approach," Presented at XIII International Symposium on Dynamic Problems of Mechanics, ABCM, Angra dos Reis, RJ, Brazil, March 2nd - March 6th, 2009.

[3] S. Savaresi, M. Tanelli, "Active Braking Control Systems Design for Vehicles", Springer London Dordrecht Heidelberg New York, 2010.

[4] C. Dantas, F. Gabriel, and R. T. Costa Neto, "Influence of the distances between the axles in the vertical dynamics of a military vehicle equipped with magnetorheological dampers," SAE Technical Paper 2018-36-0232, 2018, https://doi.org/10.4271/2018-36-0232

[5] V. W. dos Santos Belle, and R. T. Costa Neto, "Vtr 4 x 4 three-dimensional mathematical model with independent suspensions and magnetorheological dampers", SAE Technical Paper 2022-36-0036, 2023, https://doi.org/10.4271/2022-36-0036.

[6] G. B. Rangel, "Comportamento dinâmico de veículo 4×4 equipado com amortecedores magnetorreológicos trafegando sobre terreno irregular", Instituto Militar de Engenharia, 2022.

[7] The International Organization for Standardization (ISO), "Road vehicles — Vehicle dynamics and road-holding ability — Vocabulary," ISO 8855, 2011.

[8] R. N. Jazar, "Vehicle Dynamics, Theory and Application", 2nd ed., Springer Science+Business Media, LLC, DOI 10.1007/978-1-4614-8544-5, 2014.

[9] N.M. Kwok, Q.P. Ha, T.H. Nguyen, J. Li, B. Samali. "A novel hysteretic model for magnetorheological fluid dampers and parameter identification using particle swarm optimization". Elsevier, Australia, 2006.